Progress In Electromagnetics Research B, Vol. 55, 23–44, 2013

2D FDTLM HYBRIDIZATION WITH MODAL METHOD

Caroline Girard[1, 2, *], Asmaa Zugari[3], and Nathalie Raveu[1]

[1]INPT, UPS; CNRS; LAPLACE; ENSEEIHT, Université de Toulouse, 2 Rue Charles Camichel, Toulouse 31000, France

[2]NACHOS Project-Team, INRIA Sophia Antipolis-Méditerranée, 2004 Route des Lucioles, Sophia Antipolis 06560, France

[3]Electronics and Microwaves Research Group (EMG), Laboratory Systems of Information and Telecommunications (LaSIT), Faculty of Sciences, Abdelmalek Essaadi University, Av. de Sebta, Mhannech II, Tetuan 93002, Morocco

Abstract—This article focuses on the 2D hybrid technique between the Frequency Domain Transmission Line Matrix Method (FDTLM) and the Wave Concept Iterative Procedure (WCIP). 3D hybridization has already been studied, but results may be improved through a better knowledge of method order. Consequently, developing 2D hybridization aims at understanding the hybridization in simplest problems, especially because Transverse Electric (TE) and Transverse Magnetic (TM) are uncoupled. Our study dwells on accuracy and convergence order of the 2D hybrid method, which will help for 3D mesh use. In this perspective, the scattering nodes and electromagnetic fields expressions are established in the 2D general case with anisotropic materials. As a result, validation examples are presented to check the approach.

1. INTRODUCTION

Hybridizing techniques, i.e., using each technique in a part of the problem where it is the most appropriate, is an adequate way to improve the modeling of microwaves circuits. Hybrid methods have been successfully considered to study complex configurations [1–3] like inhomogeneous problems [4–7].

Received 3 June 2013, Accepted 22 September 2013, Scheduled 23 September 2013

* Corresponding author: Caroline Girard (cgirard@laplace.univ-tlse.fr).

In this work, a hybrid technique that combines two different numerical methods, the two-dimensional Frequency Domain Transmission Line Matrix Method (2D FDTLM) [8–11] and the Wave Concept Iterative Procedure method (WCIP) [12–14] is presented. The FDTLM is based on the theory of transmission lines and in the principle of propagation of light described by Huygens [8, 9, 15, 16]. The medium is discretized by transmission lines and circuits' elements in a manner that the arrangement of transmission lines and circuits' elements give equations that are isomorphic with equations of the problem, i.e., in this case, Maxwell's equations. The WCIP is an integral method based on waves' concept that solves Maxwell's equations in enclosed waveguide [17]. This technique takes advantage of the WCIP to model homogeneous media with less computational requirement (use of surface mesh and not volumic mesh) and of the ability of the FDTLM to characterize inhomogeneous media. One of the advantages of the WCIP is its ability to deal with spectral or local (spatial) sources. Furthermore, open boundary conditions are addressed by this method without adding PML conditions or radiation conditions. The hybrid algorithm is therefore based on the partition of the structure under study into two domains: the WCIP is used for the homogeneous media while the FDTLM is used for the inhomogeneous media. To simplify the hybridization, the 2D FDTLM node is reformulated using waves as used in the WCIP. In 2D, two independent orientations corresponding to TE and TM modes are distinguished. Thus, two scattering nodes are defined by either a shunt or a series matrix. Their formulation is analytically derived in this paper from Maxwell's equations using centered differencing and averaging [10, 11] as in [18] in 3D case. It is noteworthy that 2D FDTLM TM and TE matrices cannot be immediately obtained from the 3D matrix, since in each 3D development [18, 19] replacing the propagation constant along z by zero does not lead to the scattering matrix obtained in this paper.

The goal of our study is to validate 2D hybridization principles to know the properties of the method so that 3D results can be improved in accuracy compared to [19]. We want to study more complex cases as presented in Fig. 1, where the FDTLM will be applied in inhomogeneous domain containing $\varepsilon_{r,3}$ and $\varepsilon_{r,4}$ and the WCIP elsewhere. Hybrid method formulation is explained and applied in several test cases: validation of the operator spectrum, comparison with an analytical case and with diffraction by a microstrip line with homogeneous and inhomogeneous substrate. As we do not want to compete with commercial software (and moreover 2D cases cannot be dealt with them), computation times are not given.

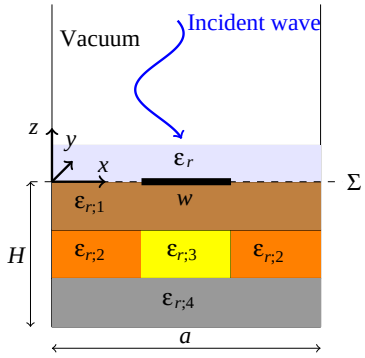

Figure 1. Complex case achievable with hybrid method.

2. HYBRID METHOD THEORY

In this section, the 2D scattering FDTLM node formulated with waves is detailed in the TE ($E_z = 0$) and TM ($H_z = 0$) cases (Transverse to z-direction). It leads to the presentation of the hybridization principle between the WCIP method and the FDTLM in Subsection 2.4.

2.1. Maxwell's Equations

Time-harmonic Maxwell's equations for invariant problem along y-axis are

$$\begin{aligned}
j\omega\varepsilon_x e_x &= -\frac{\partial h_y}{\partial z} - \sigma_{ex} e_x, \\
j\omega\varepsilon_y e_y &= \frac{\partial h_x}{\partial z} - \frac{\partial h_z}{\partial x} - \sigma_{ey} e_y, \\
j\omega\varepsilon_z e_z &= \frac{\partial h_y}{\partial x} - \sigma_{ez} e_z, \\
j\omega\mu_x h_x &= \frac{\partial e_y}{\partial z} - \sigma_{mx} h_x, \\
j\omega\mu_y h_y &= \frac{\partial e_z}{\partial x} - \frac{\partial e_x}{\partial z} - \sigma_{my} h_y, \\
j\omega\mu_z h_z &= -\frac{\partial e_y}{\partial x} - \sigma_{mz} h_z,
\end{aligned} \tag{1}$$

where ω is the pulsation. ε and μ are the permittivity and the permeability of the media. σ_e and σ_m are the electric and magnetic conductivities. e_i and h_i, $i \in \{x, y, z\}$, are the electromagnetic field components.

Let us consider an elementary cell of dimensions u, v, w respectively along the x, y, z directions. Fields are normalized according to the following transformations

$$\begin{aligned} x &= uX, \quad y = vY, \quad z = wZ, \\ e_x &= E_x/u, \quad e_y = E_y/v, \quad e_z = E_z/w, \\ h_x &= H_x/u, \quad h_y = H_y/v, \quad h_z = H_z/w. \end{aligned}$$

Normalized Maxwell's equations are obtained

$$G_{ex}E_x = -\frac{\partial H_y}{\partial Z}, \tag{2a}$$

$$G_{ey}E_y = \frac{\partial H_x}{\partial Z} - \frac{\partial H_z}{\partial X}, \tag{2b}$$

$$G_{ez}E_z = \frac{\partial H_y}{\partial X}, \tag{2c}$$

$$G_{mx}H_x = \frac{\partial E_y}{\partial Z}, \tag{2d}$$

$$G_{my}H_y = \frac{\partial E_z}{\partial X} - \frac{\partial E_x}{\partial Z}, \tag{2e}$$

$$G_{mz}H_z = -\frac{\partial E_y}{\partial X}, \tag{2f}$$

where

$$\begin{aligned} G_{ex} &= (\sigma_{ex} + j\omega\varepsilon_x)\,\frac{vw}{u}, \quad G_{mx} = (\sigma_{mx} + j\omega\mu_x)\,\frac{vw}{u}, \\ G_{ey} &= (\sigma_{ey} + j\omega\varepsilon_y)\,\frac{uw}{v}, \quad G_{my} = (\sigma_{my} + j\omega\mu_y)\,\frac{uw}{v}, \\ G_{ez} &= (\sigma_{ez} + j\omega\varepsilon_z)\,\frac{uv}{w}, \quad G_{mz} = (\sigma_{mz} + j\omega\mu_z)\,\frac{uv}{w}. \end{aligned} \tag{3}$$

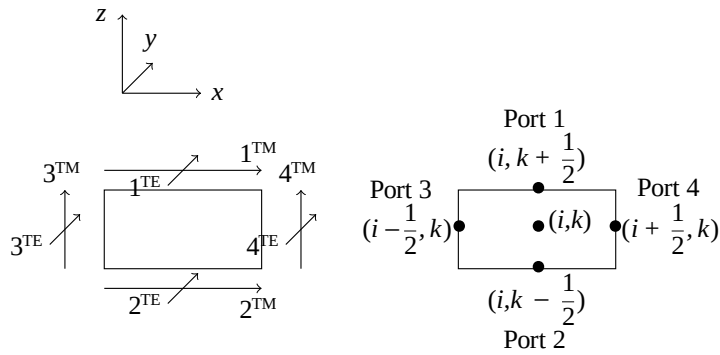

Figure 2. 2D FDTLM node in TE and TM cases.

System (2) indicates that Equations (2a), (2c) and (2e) are independent of Equations (2b), (2d) and (2f). Two independent propagation orientations are therefore studied in 2D respectively the TM modes (H_y, E_x and E_z) and the TE modes (E_y, H_x and H_z). The elementary FDTLM node is represented in Fig. 2. TE and TM indices on each node port, numbered from 1 to 4, should be considered separately since they do not coexist in 2D propagation.

2.2. TM Modes

In this case, we deal with the field components E_x, E_z and H_y. The arrangement of TM transmission lines shown in Fig. 3 can be assimilated to a series node since all waves depend on the magnetic field component H_y, but differ from the electric field components E_x and E_z. Maxwell's equations concerned in the TM case are Equations (2a), (2c) and (2e). Centered differencing at point (i, k) is achieved on these equations, leading to finite difference equations

$$G_{ex}E_x(i,k) = H_y\left(i, k-\frac{1}{2}\right) - H_y\left(i, k+\frac{1}{2}\right), \tag{4}$$

$$G_{ez}E_z(i,k) = H_y\left(i+\frac{1}{2}, k\right) - H_y\left(i-\frac{1}{2}, k\right), \tag{5}$$

$$\begin{aligned} G_{my}H_y(i,k) = {} & E_z\left(i+\frac{1}{2}, k\right) - E_z\left(i-\frac{1}{2}, k\right), \\ & + E_x\left(i, k-\frac{1}{2}\right) - E_x\left(i, k+\frac{1}{2}\right). \end{aligned} \tag{6}$$

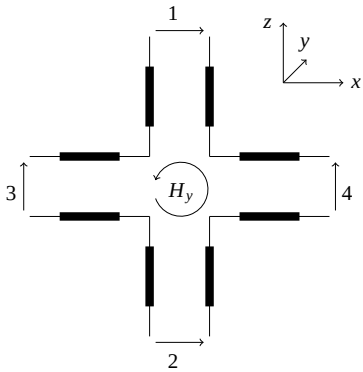

Figure 3. Representation of the 2D series FDTLM node.

2.2.1. Wave Definition on a Series FDTLM Node

Incident and reflected waves, noted A_l and B_l, are defined on the FDTLM node port numbered l at the sampling points defined according to notation of Fig. 2. Writing waves on port 1 means considering fields at mesh point $(i, k + \frac{1}{2})$. Given waves definitions provided in [13], we obtain

$$\begin{aligned} \mathbf{A_1} &= \frac{1}{2\sqrt{Z_0}} \left[\mathbf{E}\left(i, k+\frac{1}{2}\right) + Z_0 \mathbf{J}\left(i, k+\frac{1}{2}\right) \right], \\ \mathbf{B_1} &= \frac{1}{2\sqrt{Z_0}} \left[\mathbf{E}\left(i, k+\frac{1}{2}\right) - Z_0 \mathbf{J}\left(i, k+\frac{1}{2}\right) \right]. \end{aligned} \tag{7}$$

Projecting on x-axis, we obtain

$$\begin{aligned} A_1 &= \frac{1}{2\sqrt{Z_0}} \left[E_x\left(i, k+\frac{1}{2}\right) + Z_0 J_x\left(i, k+\frac{1}{2}\right) \right], \\ B_1 &= \frac{1}{2\sqrt{Z_0}} \left[E_x\left(i, k+\frac{1}{2}\right) - Z_0 J_x\left(i, k+\frac{1}{2}\right) \right], \end{aligned} \tag{8}$$

where Z_0 is the free space impedance and

$$\mathbf{J} = \mathbf{H} \wedge (-\mathbf{z}),$$

with $\wedge$ the vector product and thus

$$J_x\left(i, k+\frac{1}{2}\right) = -H_y\left(i, k+\frac{1}{2}\right),$$

which entails

$$\begin{aligned} A_1 &= \frac{1}{2\sqrt{Z_0}} \left[E_x\left(i, k+\frac{1}{2}\right) - Z_0 H_y\left(i, k+\frac{1}{2}\right) \right], \\ B_1 &= \frac{1}{2\sqrt{Z_0}} \left[E_x\left(i, k+\frac{1}{2}\right) + Z_0 H_y\left(i, k+\frac{1}{2}\right) \right]. \end{aligned} \tag{9}$$

Relations (9) transform the normalized field components to incident and reflected waves at port 1. Waves at the other ports are found in a similar way, they are reported in Appendix A.1.

2.2.2. Field Definition on Series FDTLM Node

Electromagnetic fields are expressed by combining Equation (9)

$$\begin{aligned} E_x\left(i, k+\frac{1}{2}\right) &= \sqrt{Z_0}\,(A_1 + B_1), \\ H_y\left(i, k+\frac{1}{2}\right) &= \frac{1}{\sqrt{Z_0}}\,(B_1 - A_1). \end{aligned} \tag{10}$$

Fields at the other ports are found similarly, they are provided in Appendix A.2. By substituting (10) into (4)–(6), the following equations are deduced:

$$G_{ex}E_x\left(i,k\right)=\frac{1}{\sqrt{Z_0}}\left(A_1-B_1+A_2-B_2\right), \tag{11}$$

$$G_{ez}E_z\left(i,k\right)=\frac{1}{\sqrt{Z_0}}\left(A_4-B_4+A_3-B_3\right), \tag{12}$$

$$G_{my}H_y\left(i,k\right)=\sqrt{Z_0}(A_4+B_4-A_3-B_3-A_1-B_1+A_2+B_2). \tag{13}$$

2.2.3. Averaging the Field Component Combinations

The next step is to express the field component combinations at the central point $(i,\ k)$ as a combination of the incident and reflected waves of surrounding ports. Since z-axis is orthogonal to both E_x and H_y, the combination $(E_x - Z_0H_y)$ is centered averaged at the central point $(i,\ k)$ with respect to this direction:

$$E_x\left(i,k\right)-Z_0H_y\left(i,k\right)=\frac{1}{2}\begin{pmatrix}E_x\left(i,k+\frac{1}{2}\right)-Z_0H_y\left(i,k+\frac{1}{2}\right)\\+E_x\left(i,k-\frac{1}{2}\right)-Z_0H_y\left(i,k-\frac{1}{2}\right)\end{pmatrix}. \tag{14}$$

Substituting field definitions of Appendix A.2 into (14) leads to

$$E_x\left(i,k\right)-Z_0H_y\left(i,k\right)=\frac{1}{2}\begin{pmatrix}\sqrt{Z_0}(A_1+B_1)-Z_0\frac{1}{\sqrt{Z_0}}(B_1-A_1)\\+\sqrt{Z_0}(A_2+B_2)-Z_0\frac{1}{\sqrt{Z_0}}(A_2-B_2)\end{pmatrix} \tag{15}$$

$$E_x\left(i,k\right)-Z_0H_y\left(i,k\right)\ =\sqrt{Z_0}\left(A_1+B_2\right). \tag{16}$$

Similarly, the centered average for other combinations at the central point $(i,\ k)$, namely $(E_x + Z_0H_y)$, $(E_z - Z_0H_y)$ and $(E_z + Z_0H_y)$ are reported in Appendix A.3. From these relations, reflected waves B at each port are deduced from incident waves A and electromagnetic fields at the center of the node

$$B_1+B_2=\frac{2E_x(i,k)}{\sqrt{Z_0}}-(A_1+A_2). \tag{17}$$

This definition is introduced in (11) to obtain E_x at the central point $(i,\ k)$

$$E_x\left(i,k\right)=\frac{2\sqrt{Z_0}}{\left(Z_0G_{ex}+2\right)}\left(A_1+A_2\right). \tag{18}$$

By the same way, we obtain field components E_z and H_y at the central point (i,k)

$$E_z\left(i,k\right)=\frac{2\sqrt{Z_0}}{\left(Z_0G_{ez}+2\right)}\left(A_3+A_4\right), \tag{19}$$

$$H_y(i,k) = \frac{2\sqrt{Z_0}}{(4Z_0 + G_{my})}(A_4 - A_3 + A_2 - A_1). \tag{20}$$

Finally, the scattering matrix of the series node is a 4×4 matrix

$$S_e = \begin{pmatrix} a_{xy} & c_{xy} & -b_y & b_y \\ c_{xy} & a_{xy} & b_y & -b_y \\ -b_y & b_y & a_{zy} & c_{zy} \\ b_y & -b_y & c_{zy} & a_{zy} \end{pmatrix}, \tag{21}$$

where index e stands for the element, i.e., the FDTLM node and

$$\begin{aligned} a_{\alpha,\beta} &= d_\alpha - b_\beta, \quad b_\beta = \frac{2Z_0}{(4Z_0 + G_{m\beta})}, \\ c_{\alpha,\beta} &= b_\beta + d_\alpha - 1, \quad d_\alpha = \frac{2}{(2 + Z_0 G_{e\alpha})}, \end{aligned} \tag{22}$$

with $\alpha = x, z$ and $\beta = y$.

2.3. TE Modes

In this case, we deal with the field components H_x, H_z and E_y. The arrangement of TE transmission lines shown in Fig. 4 can be assimilated to a shunt node since all waves depend on the electric field component E_y, but differ from the magnetic field components H_x and H_z. Maxwell's equations concerned in the TE case are Equations (2b), (2d) and (2f). Centered differencing at point (i, k) is achieved on these equations, leading to finite difference equations

$$\begin{aligned} G_{ey} E_y(i,k) = {} & H_x\left(i, k + \frac{1}{2}\right) - H_x\left(i, k - \frac{1}{2}\right) \\ & + H_z\left(i - \frac{1}{2}, k\right) - H_z\left(i + \frac{1}{2}, k\right), \end{aligned} \tag{23}$$

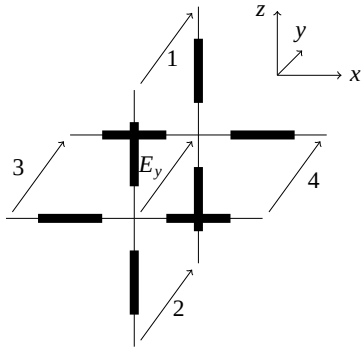

Figure 4. Representation of 2D shunt FDTLM node.

$$G_{mx}H_x\left(i,k\right)=E_y\left(i,k+\frac{1}{2}\right)-E_y\left(i,k-\frac{1}{2}\right), \tag{24}$$

$$G_{mz}H_z\left(i,k\right)=E_y\left(i-\frac{1}{2},k\right)-E_y\left(i+\frac{1}{2},k\right). \tag{25}$$

Wave and field definitions are detailed in Appendix B.1 and B.2. By substituting these equations into (23)–(25), the following equations are deduced:

$$\begin{aligned} G_{ey}E_y\left(i,k\right) &= \frac{1}{\sqrt{Z_0}}(A_1-B_1+A_2-B_2 \\ &\quad +A_3-B_3+A_4-B_4), \end{aligned} \tag{26}$$

$$G_{mx}H_x\left(i,k\right)=\sqrt{Z_0}\left(A_1+B_1-A_2-B_2\right), \tag{27}$$

$$G_{mz}H_z\left(i,k\right)=\sqrt{Z_0}\left(A_3+B_3-A_4-B_4\right). \tag{28}$$

Centered averaging electromagnetic field combinations at the center of the node is detailed in Appendix B.3. Expressions of field components at the central point $(i,\ k)$ are obtained similarly as TM case

$$E_y\left(i,k\right)=\frac{2\sqrt{Z_0}}{\left(Z_0G_{ey}+4\right)}\left(A_1+A_2+A_3+A_4\right), \tag{29}$$

$$H_x\left(i,k\right)=\frac{2\sqrt{Z_0}}{\left(2Z_0+G_{mx}\right)}\left(A_1-A_2\right), \tag{30}$$

$$H_z\left(i,k\right)=\frac{2\sqrt{Z_0}}{\left(2Z_0+G_{mz}\right)}\left(A_3-A_4\right). \tag{31}$$

Consequently, the scattering matrix of the shunt node is a 4×4 matrix

$$S_e=\begin{pmatrix} a_{yx} & c_{yx} & d_y & d_y \\ c_{yx} & a_{yx} & d_y & d_y \\ d_y & d_y & a_{yz} & c_{yz} \\ d_y & d_y & c_{yz} & a_{yz} \end{pmatrix}, \tag{32}$$

where

$$\begin{aligned} a_{\alpha,\beta}&=d_\alpha-b_\beta,\quad b_\beta=\frac{2Z_0}{\left(2Z_0+G_{m\beta}\right)}, \\ c_{\alpha,\beta}&=b_\beta+d_\alpha-1,\quad d_\alpha=\frac{2}{\left(4+Z_0G_{e\alpha}\right)}, \end{aligned} \tag{33}$$

with $\beta=z,\ x$ and $\alpha=y$.

2.4. WCIP/FDTLM Hybrid System

The WCIP is adapted to homogeneous planar circuits and implies only line mesh in this case. If homogeneous substrates are considered, results can be obtained with the WCIP alone. The WCIP method implemented in this particular case may therefore be used as a reference to validate the WCIP/FDTLM hybrid method results. The general case of study is represented in Fig. 5, where an interface (Σ) separates the two partitions of the domain.

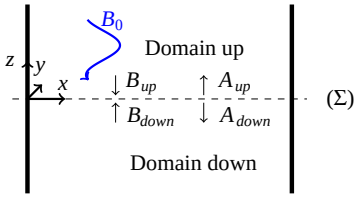

Figure 5. Representation of the studied case, separation between the upper and lower media according to the interface (Σ).

When hybrid method is considered, the media under the surface (Σ) is discretized by the FDTLM (2D mesh of the whole lower media) while the upper media is always characterized by the WCIP operator. Transfer condition is provided through the S operator of the WCIP. A_{down} corresponds to A_1 of the upper nodes of the 2D FDTLM mesh and B_1 corresponds to B_{down} of the system. B_{down} comes from the FDTLM application according to (21) in TM case and (32) in TE case. With a spectral source wave B_0 in the upper media, the equations to consider are

$$\begin{pmatrix} B_{up} \\ B_{down} \end{pmatrix} = \begin{pmatrix} S_{up}^{\mathrm{W}} & 0 \\ 0 & S_{down}^{\mathrm{F}} \end{pmatrix} \begin{pmatrix} A_{up} \\ A_{down} \end{pmatrix} + \begin{pmatrix} B_0 \\ 0 \end{pmatrix}, \tag{34}$$

$$\begin{pmatrix} A_{up} \\ A_{down} \end{pmatrix} = S \begin{pmatrix} B_{up} \\ B_{down} \end{pmatrix}, \tag{35}$$

where the exponents W and F stand for WCIP and FDTLM, the operator S contains the transmission/reflection conditions on (Σ), and $(S_i^{\mathrm{W}})_{i=up,down}$ are the scattering operators for homogeneous media in domain i. The discrete operators $(S_i^{\mathrm{W}})_{i=up,down}$ are based on the Fast Modal Transform (FMT) [12–14] and on the modal scattering operator $(\hat{\Gamma}_i)$ according to

$$S_i^{\mathrm{W}} = \mathrm{FMT}^{-1}\hat{\Gamma}_i\mathrm{FMT}. \tag{36}$$

(FMT) expresses the waves from the spatial domain to modal domain. If $\mathbf{B}$ is the incident wave, its associated modal decomposition

($\{\tilde{B_n}\}_{n\in[\![0;N-1]\!]}$) and spatial decomposition ($\{B_k\}_{k\in[\![0;N-1]\!]}$) are expressed through

$$\mathbf{B} = \sum_n \tilde{B_n}\mathbf{f_n} = \sum_k B_k \mathbf{H_k} \tag{37}$$

where k is the segment position in the spatial basis, ($\{\mathbf{H_k}\}_{\mathbf{k}\in[\![\mathbf{0};\mathbf{N-1}]\!]}$), and n the mode order in the modal basis, ($\{\mathbf{f_n}\}_{\mathbf{n}\in[\![\mathbf{0};\mathbf{N-1}]\!]}$).

Its modal decomposition is obtained thanks to FMT writing

$$\tilde{B_n} = \langle \mathbf{f_n}, \mathbf{B}\rangle = \left\langle \mathbf{f_n}, \sum_k B_k \mathbf{H_k} \right\rangle. \tag{38}$$

These bases verify

$$\begin{aligned} \langle \mathbf{H_{k_1}}, \mathbf{H_{k_2}}\rangle &= \delta_{k_1,k_2}, \\ \langle \mathbf{f_{n_1}}, \mathbf{f_{n_2}}\rangle &= \delta_{n_1,n_2}. \end{aligned} \tag{39}$$

Γ_i is the modal coefficient of diffraction. Its expression is given by

$$\Gamma_i = \frac{1 - Z_0 Y_i}{1 + Z_0 Y_i}, \tag{40}$$

with Y_i detailed in (41) in TE case, in (42) in TM case

$$Y_i^{\mathrm{TE}} = \frac{\sqrt{\left(\frac{i\pi}{a}\right)^2 - k_0^2}}{j\omega\mu_0}, \tag{41}$$

$$Y_i^{\mathrm{TM}} = \frac{j\omega\varepsilon_0}{\sqrt{\left(\frac{i\pi}{a}\right)^2 - k_0^2}}, \tag{42}$$

where i is the index of the mode taken into account in the matrix. S links incident and reflected waves with

$$\mathbf{A} = S\mathbf{B} = \begin{pmatrix} S_{11} & S_{12} \\ S_{21} & S_{22} \end{pmatrix} \mathbf{B} \tag{43}$$

with

$$S_{11} = -\sum_{k_1,k_2} \left| H_{k_1}^{\mathrm{metal}} \right\rangle \left\langle H_{k_2}^{\mathrm{metal}} \right| = S_{22}, \tag{44}$$

and

$$S_{12} = \sum_{k_1,k_2} \left| H_{k_1}^{\mathrm{insulator}} \right\rangle \left\langle H_{k_2}^{\mathrm{insulator}} \right| = S_{21}. \tag{45}$$

Combining (34) and (35), the linear system to solve in the hybrid method is

$$\left(\mathrm{I_d} - \begin{pmatrix} S_{up}^{\mathrm{W}} & 0 \\ 0 & S_{down}^{\mathrm{F}} \end{pmatrix} S \right) \begin{pmatrix} B_{up} \\ B_{down} \end{pmatrix} = \begin{pmatrix} B_0 \\ 0 \end{pmatrix}, \tag{46}$$

where $\mathrm{I_d}$ is the identity matrix. Note that when the TE case is considered, B_0 is along the y-axis and in the TM case, B_0 is along the x-axis. In 2D, TE and TM modes are uncoupled which entails that the generated waves are directed along the same axis as the source wave B_0.

3. NUMERICAL RESULTS

3.1. Mode Diffraction on a Perfect Conductor Sheet

To validate the method, the propagation of one (TE or TM) mode in vacuum ($\varepsilon_r = 1$) between two metallic slabs separated by a distance a ended by a short circuit at distance H is first considered (Fig. 6).

The solution is defined by (47) [20].

$$\begin{aligned} \mathbf{E}(x,z) &= E_0 \left[2\sinh\left(p_1(H+z)\right) e^{-p_1 H} \mathbf{f}_1^{\alpha} \right], \text{ with} \\ p_1 &= \sqrt{\left(\frac{\pi}{a}\right)^2 - k_0^2} \\ \mathbf{f}_1^{\mathrm{TE}} &= \sqrt{\frac{2}{a}} \sin\left(\frac{\pi x}{a}\right) \mathbf{y} \quad \text{and} \quad \mathbf{f}_1^{\mathrm{TM}} = \sqrt{\frac{2}{a}} \cos\left(\frac{\pi x}{a}\right) \mathbf{x} \end{aligned} \tag{47}$$

where E_0 is the incident wave amplitude, $\mathbf{y}$ and $\mathbf{x}$ the unit vectors of the canonical basis, $\mathbf{f}_1^{\alpha}$ the function of order 1 of the modal basis of the mode α (α = TE or TM), and p_1 the propagation constant along the z-axis. Here $a = 1.27\,\mathrm{cm}$, $H = 1.27\,\mathrm{cm}$ and the working frequency is 16 GHz, which implies that the modes in excitation which

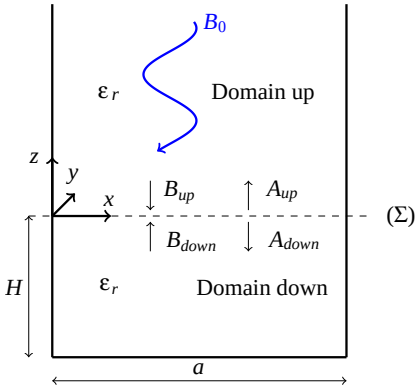

Figure 6. Mode diffraction on a perfect conductor sheet.

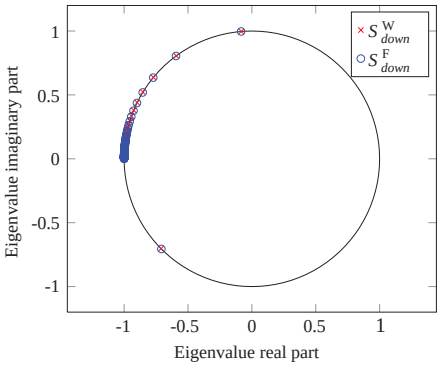

Figure 7. Eigenvalues of S_{down} for $N = 32$.

are either TE_1, either TM_1, are propagating. Eigenvalues of S^{W}_{down} and S^{F}_{down} operators are compared and represented in Fig. 7 in the TE case, where N denotes the number of segments on the interface (Σ) and consequently the number of nodes in x direction (see Fig. 2). We take the same number of nodes in z direction. The distance between both operators (norm 2) is presented in Table 1 for the TE and TM cases. Mesh size represents edge length ratio between current and initial mesh. For instance, 1/2 means that the step size is twice smaller than the initial step size in both axes. Initial mesh is characterized by a step size of 794 µm in both directions and by $N = 16$ for the FDTLM.

Since the analytical solution is known, we can calculate relative discretization error, i.e., error between analytical and computed solutions with the hybrid method. This error is evaluated and reported in Table 2 where the exponents H and $\mathrm{E_x}$ stand for Hybrid and Exact. Convergence order is estimated taking into account the errors from two consecutive mesh sizes, which explains the empty boxes of the tables, and is close to 2. Its definition is given by

$$\mathrm{Order} = \frac{\log(\mathrm{Rel\_error}(h_1)) - \log(\mathrm{Rel\_error}(h_2))}{\log(h_1) - \log(h_2)} \tag{48}$$

where $\mathrm{Rel\_error}(h_1)$ and $\mathrm{Rel\_error}(h_2)$ correspond to the relative discretization errors in L_2-norm for mesh step h_1 and refined mesh

Table 1. $||S^{\mathrm{W}}_{down} - S^{\mathrm{F}}_{down}||_2$ in TE and TM cases.

Mesh size	TE case	TM case
1	$1.693.10^{-1}$	$1.544.10^{-1}$
1/2	$8.467.10^{-2}$	$8.085.10^{-2}$
1/4	$4.233.10^{-2}$	$4.137.10^{-2}$
1/8	$2.116.10^{-2}$	$2.092.10^{-2}$
1/16	$1.058.10^{-2}$	$1.052.10^{-2}$

Table 2. Relative error on E-fields on (Σ) for TE and TM cases.

Mesh size	N	$\left\| \frac{\mathbf{E}^{\mathrm{H,TE}} - \mathbf{E}^{\mathrm{E_x,TE}}}{\max\lvert\mathbf{E}^{\mathrm{E_x,TE}}\rvert} \right\|_{L^2}$		$\left\| \frac{\mathbf{E}^{\mathrm{H,TM}} - \mathbf{E}^{\mathrm{E_x,TM}}}{\max\lvert\mathbf{E}^{\mathrm{E_x,TM}}\rvert} \right\|_{L^2}$	
		Error	Order	Error	Order
1	16	$5.92.10^{-3}$	-	$5.28.10^{-3}$	-
1/2	32	$1.47.10^{-3}$	2.0068	$1.32.10^{-3}$	1.9983
1/4	64	$3.68.10^{-4}$	2.0017	$3.31.10^{-4}$	1.9996
1/8	128	$9.19.10^{-5}$	2.0004	$8.27.10^{-5}$	1.9999
1/16	256	$2.30.10^{-5}$	2.0001	$2.07.10^{-5}$	2.0000

step h_2. The same study was performed between analytical solution and the WCIP alone and the error was of the order of the machine accuracy, which means that the WCIP is analytical in this case.

The same work was achieved with TM modes. Relative discretization error is represented in Fig. 8. It is calculated while refining the mesh along both axis (x and z-axis). Error is slightly smaller for TM modes than TE ones.

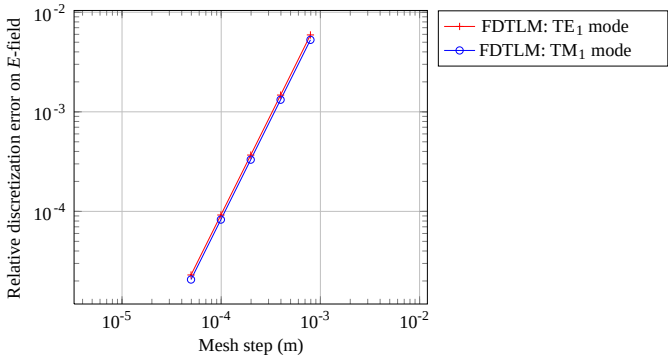

Figure 8. Relative discretization error in L_2-norm for E field with TE_1 or TM_1 in excitation.

3.2. Mode Diffraction on a Microstrip Line

A second test problem is considered (see Fig. 9). It consists of a centered metallic (perfect conductor) microstrip line of width $w = 6.35\,\text{mm}$, taken without thickness, which is inserted on the surface (Σ). Domains up and down are vacuum ($\varepsilon_r = 1$). Like previously, we have metallic boundary conditions on $x = 0$, $x = a$ and $z = -H$, with $a = 1.27\,\text{cm}$ and $H = 1.27\,\text{cm}$.

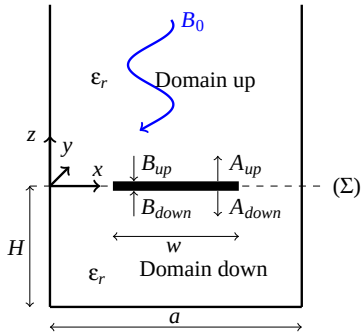

Figure 9. Representation of the microstrip line.

A comparison between the electric field and the electric current obtained with the WCIP alone (denoted by the index W) and with the hybrid method is presented as an analytical solution is not known in this particular case. The WCIP alone is meshed enough to consider it as a reference solution (the WCIP is meshed with $N = 2^{15}$ where N is the number of segments on (Σ)). Results obtained for TE_1 and TM_1 excitation are respectively detailed in Tables 3 and 4. In TE case, convergence orders of 1 and 0.5 are found for the electric field and the electric current, while in TM case convergence orders of 0.5 and 1 are respectively found for the electric field and the electric current.

Table 3. TE case: relative error on the tangential electric field and on the current on (Σ).

Mesh size	N	$\left\| \frac{\mathbf{E}^{\mathrm{H}}-\mathbf{E}^{\mathrm{W}}}{\max\lvert\mathbf{E}^{\mathrm{W}}\rvert} \right\|_{L^2}$		$\left\| \frac{\mathbf{J}^{\mathrm{H}}-\mathbf{J}^{\mathrm{W}}}{\max\lvert\mathbf{J}^{\mathrm{W}}\rvert} \right\|_{L^2}$	
		Error	Order	Error	Order
1	16	$2.65.10^{-2}$	-	$2.73.10^{-2}$	-
1/2	32	$1.47.10^{-2}$	0.8557	$1.91.10^{-2}$	0.5142
1/4	64	$7.72.10^{-3}$	0.9237	$1.33.10^{-2}$	0.5212
1/8	128	$4.06.10^{-3}$	0.9262	$9.22.10^{-3}$	0.5308
1/16	256	$2.11.10^{-3}$	0.9440	$6.32.10^{-3}$	0.5435

Table 4. TM case: relative error on the tangential electric field and on the current on (Σ).

Mesh size	N	$\left\| \frac{\mathbf{E}^{\mathrm{H}}-\mathbf{E}^{\mathrm{W}}}{\max\lvert\mathbf{E}^{\mathrm{W}}\rvert} \right\|_{L^2}$		$\left\| \frac{\mathbf{J}^{\mathrm{H}}-\mathbf{J}^{\mathrm{W}}}{\max\lvert\mathbf{J}^{\mathrm{W}}\rvert} \right\|_{L^2}$	
		Error	Order	Error	Order
1	16	$2.73.10^{-2}$	-	$2.95.10^{-2}$	-
1/2	32	$1.91.10^{-2}$	0.5106	$1.55.10^{-2}$	0.9252
1/4	64	$1.34.10^{-2}$	0.5187	$8.07.10^{-3}$	0.9450
1/8	128	$9.26.10^{-3}$	0.5287	$4.22.10^{-3}$	0.9345
1/16	256	$6.36.10^{-3}$	0.5423	$2.19.10^{-3}$	0.9486

3.3. Mode Diffraction on a Microstrip Line with Inhomogeneous Substrate

A last test problem is considered (see Fig. 10). It consists of a centered metallic (perfect conductor) microstrip line of width $w = 6.35\,\mathrm{mm}$, taken without thickness, which is inserted on the surface (Σ) of an

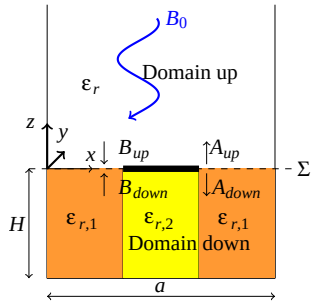

Figure 10. Representation of the microstrip line above an inhomogeneous substrate.

Table 5. TE case: relative error on the tangential electric field and on the current on (Σ).

Mesh size	N	$\left\| \frac{\mathbf{E}^{\mathrm{H}}-\mathbf{E}^{\mathrm{FEM}}}{\max\lvert\mathbf{E}^{\mathrm{FEM}}\rvert} \right\|_{L^2}$		$\left\| \frac{\mathbf{J}^{\mathrm{H}}-\mathbf{J}^{\mathrm{FEM}}}{\max\lvert\mathbf{J}^{\mathrm{FEM}}\rvert} \right\|_{L^2}$	
		Error	Order	Error	Order
1	16	$2.48.10^{-2}$	-	$2.06.10^{-2}$	-
1/2	32	$1.34.10^{-2}$	0.8824	$1.39.10^{-2}$	0.5725
1/4	64	$6.87.10^{-3}$	0.9689	$8.97.10^{-3}$	0.6296
1/8	128	$3.40.10^{-3}$	1.0145	$5.47.10^{-3}$	0.7126
1/16	256	$1.56.10^{-3}$	1.1222	$3.07.10^{-3}$	0.8366

inhomogeneous substrate ($\varepsilon_{r,1} = 1$ and $\varepsilon_{r,2} = 5$). Domain up is vacuum ($\varepsilon_r = 1$). Like previously, we have metallic boundary conditions on $x = 0$, $x = a$ and $z = -H$, with $a = 1.27\,\mathrm{cm}$ and $H = 1.27\,\mathrm{cm}$.

A comparison between the electric field and the electric current obtained with an hybrid WCIP/FEM method [21] taken as our reference is presented, meshing this hybrid method with $N = 2^{10}$, since an analytical solution is not known. Results obtained for TE_1 excitation are detailed in Table 5. In TE case, convergence orders of 1 and 0.5 are found for the electric field and the electric current, while in TM case convergence orders of 0.5 and 1 are respectively found for the electric field and the electric current.

4. CONCLUSION

The 2D FDTLM node reformulated for hybridization with the WCIP is detailed in this paper in the TE and TM cases. The hybrid FDTLM/WCIP formulation is expressed and tested in an

analytical case and in two microstrip line cases (homogeneous and inhomogeneous). In this analytical case (diffraction of one guided mode on a perfect sheet), the spectra of both scattering operators are successfully compared. In the microstrip line case, the method order is 1 (resp. 0.5) on the electric field and 0.5 (resp. 1) on the electric current for TE modes (resp. for TM modes) for homogeneous and inhomogeneous examples. Similar works are under process with other volumic methods such as Finite Element Method (FEM) or a Hybridizable Discontinuous Galerkin (HDG) method [22].

ACKNOWLEDGMENT

The authors would like to thank the Defence Procurement Agency (DGA) which supports the first author.

APPENDIX A. DEVELOPMENTS IN TM CASE

A.1. Wave Definition

Incident and reflected waves are detailed at each port of the series FDTLM node:

$$A_1 = \frac{1}{2\sqrt{Z_0}}\left(E_x\left(i,k+\frac{1}{2}\right) - Z_0 H_y\left(i,k+\frac{1}{2}\right)\right),$$

$$B_1 = \frac{1}{2\sqrt{Z_0}}\left(E_x\left(i,k+\frac{1}{2}\right) + Z_0 H_y\left(i,k+\frac{1}{2}\right)\right),$$

$$A_2 = \frac{1}{2\sqrt{Z_0}}\left(E_x\left(i,k-\frac{1}{2}\right) + Z_0 H_y\left(i,k-\frac{1}{2}\right)\right),$$

$$B_2 = \frac{1}{2\sqrt{Z_0}}\left(E_x\left(i,k-\frac{1}{2}\right) - Z_0 H_y\left(i,k-\frac{1}{2}\right)\right),$$

$$A_3 = \frac{1}{2\sqrt{Z_0}}\left(E_z\left(i-\frac{1}{2},k\right) - Z_0 H_y\left(i-\frac{1}{2},k\right)\right),$$

$$B_3 = \frac{1}{2\sqrt{Z_0}}\left(E_z\left(i-\frac{1}{2},k\right) + Z_0 H_y\left(i-\frac{1}{2},k\right)\right),$$

$$A_4 = \frac{1}{2\sqrt{Z_0}}\left(E_z\left(i+\frac{1}{2},k\right) + Z_0 H_y\left(i+\frac{1}{2},k\right)\right),$$

$$B_4 = \frac{1}{2\sqrt{Z_0}}\left(E_z\left(i+\frac{1}{2},k\right) - Z_0 H_y\left(i+\frac{1}{2},k\right)\right).$$

A.2. Field Definition

Electromagnetic fields are deduced from wave definitions at each port of the series FDTLM node:

$$E_x\left(i,k+\frac{1}{2}\right)=\sqrt{Z_0}\,(A_1+B_1)\,,$$
$$H_y\left(i,k+\frac{1}{2}\right)=\frac{1}{\sqrt{Z_0}}\,(B_1-A_1)\,,$$
$$E_x\left(i,k-\frac{1}{2}\right)=\sqrt{Z_0}\,(A_2+B_2)\,,$$
$$H_y\left(i,k-\frac{1}{2}\right)=\frac{1}{\sqrt{Z_0}}\,(A_2-B_2)\,,$$
$$E_z\left(i-\frac{1}{2},k\right)=\sqrt{Z_0}\,(A_3+B_3)\,,$$
$$H_y\left(i-\frac{1}{2},k\right)=\frac{1}{\sqrt{Z_0}}\,(B_3-A_3)\,,$$
$$E_z\left(i+\frac{1}{2},k\right)=\sqrt{Z_0}\,(A_4+B_4)\,,$$
$$H_y\left(i+\frac{1}{2},k\right)=\frac{1}{\sqrt{Z_0}}\,(A_4-B_4)\,.$$

A.3. Centered Average for the Field Component Combinations

$$E_x\,(i,k)+Z_0H_y\,(i,k)=\sqrt{Z_0}\,(A_2+B_1)$$
$$E_x\,(i,k)-Z_0H_y\,(i,k)=\sqrt{Z_0}\,(A_1+B_2)$$
$$E_z\,(i,k)+Z_0H_y\,(i,k)=\sqrt{Z_0}\,(A_4+B_3)$$
$$E_z\,(i,k)-Z_0H_y\,(i,k)=\sqrt{Z_0}\,(A_3+B_4)$$

APPENDIX B. DEVELOPMENTS IN TE CASE

B.1. Wave Definition

Incident and reflected waves are detailed at each port of the shunt FDTLM node:

$$A_1=\frac{1}{2\sqrt{Z_0}}\left(E_y\left(i,k+\frac{1}{2}\right)+Z_0H_x\left(i,k+\frac{1}{2}\right)\right),$$

$$B_1 = \frac{1}{2\sqrt{Z_0}}\left(E_y\left(i,k+\frac{1}{2}\right) - Z_0 H_x\left(i,k+\frac{1}{2}\right)\right),$$
$$A_2 = \frac{1}{2\sqrt{Z_0}}\left(E_y\left(i,k-\frac{1}{2}\right) - Z_0 H_x\left(i,k-\frac{1}{2}\right)\right),$$
$$B_2 = \frac{1}{2\sqrt{Z_0}}\left(E_y\left(i,k-\frac{1}{2}\right) + Z_0 H_x\left(i,k-\frac{1}{2}\right)\right),$$
$$A_3 = \frac{1}{2\sqrt{Z_0}}\left(E_y\left(i-\frac{1}{2},k\right) + Z_0 H_z\left(i-\frac{1}{2},k\right)\right),$$
$$B_3 = \frac{1}{2\sqrt{Z_0}}\left(E_y\left(i-\frac{1}{2},k\right) - Z_0 H_z\left(i-\frac{1}{2},k\right)\right),$$
$$A_4 = \frac{1}{2\sqrt{Z_0}}\left(E_y\left(i+\frac{1}{2},k\right) - Z_0 H_z\left(i+\frac{1}{2},k\right)\right),$$
$$B_4 = \frac{1}{2\sqrt{Z_0}}\left(E_y\left(i+\frac{1}{2},k\right) + Z_0 H_z\left(i+\frac{1}{2},k\right)\right).$$

B.2. Field Definition

Electromagnetic fields are deduced from wave definitions at each port of the shunt FDTLM node:

$$E_y\left(i,k+\frac{1}{2}\right) = \sqrt{Z_0}\,(A_1+B_1),$$
$$H_x\left(i,k+\frac{1}{2}\right) = \frac{1}{\sqrt{Z_0}}\,(A_1-B_1),$$
$$E_y\left(i,k-\frac{1}{2}\right) = \sqrt{Z_0}\,(A_2+B_2),$$
$$H_x\left(i,k-\frac{1}{2}\right) = \frac{1}{\sqrt{Z_0}}\,(B_2-A_2),$$
$$E_y\left(i-\frac{1}{2},k\right) = \sqrt{Z_0}\,(A_3+B_3),$$
$$H_z\left(i-\frac{1}{2},k\right) = \frac{1}{\sqrt{Z_0}}\,(A_3-B_3),$$
$$E_y\left(i+\frac{1}{2},k\right) = \sqrt{Z_0}\,(A_4+B_4),$$
$$H_z\left(i+\frac{1}{2},k\right) = \frac{1}{\sqrt{Z_0}}\,(B_4-A_4).$$

B.3. Centered Average for the Field Component Combinations

$$E_y(i,k) + Z_0 H_x(i,k) = \sqrt{Z_0}(A_1 + B_2)$$
$$E_y(i,k) - Z_0 H_x(i,k) = \sqrt{Z_0}(A_2 + B_1)$$
$$E_y(i,k) + Z_0 H_z(i,k) = \sqrt{Z_0}(A_3 + B_4)$$
$$E_y(i,k) - Z_0 H_z(i,k) = \sqrt{Z_0}(A_4 + B_3)$$

REFERENCES

1. Taflove, A. and K. Umashankar, "A hybrid moment method/finite-difference time-domain approach to electromagnetic coupling and aperture penetration into complex geometries," *IEEE Transactions on Antennas and Propagation*, Vol. 30, No. 4, 617–627, Jul. 1982.
2. Paulsen, K. D., D. R. Lynch, and J. W. Strohbehn, "Three-dimensional finite, boundary, and hybrid elements solutions of the Maxwell equations for lossy dielectric media," *IEEE Transactions on Microwave Theory and Techniques*, Vol. 36, No. 4, 682–693, Apr. 1988.
3. Sroka, J., H. Baggenstos, and R. Ballisti, "On the coupling of the generalized multipole technique with the finite element method," *IEEE Transactions on Magnetics*, Vol. 26, No. 2, 658–661, Mar. 1990.
4. Yuan, X. C., D. R. Lynch, and J. W. Strohbehn, "Coupling of finite element and moment methods for electromagnetic scattering from inhomogeneous objects," *IEEE Transactions on Antennas and Propagation*, Vol. 38, No. 3, 386–393, Mar. 1990.
5. Yuan, X. C., "Three-dimensional electromagnetic scattering from inhomogeneous objects by the hybrid moment and finite element method," *IEEE Transactions on Microwave Theory and Techniques*, Vol. 38, No. 8, 1053–1058, Aug. 1990.
6. Boyse, W. E. and A. A. Seidl, "A hybrid finite element and moment method for electromagnetic scattering from inhomogeneous objects," *Proceeding of the 7th Annual Review of Progress in Applied Computational Electromagnetics*, 160–169, Mar. 1991.
7. Yuan, X. C., D. R. Lynch, and K. D. Paulsen, "Importance of normal field continuity in inhomogeneous scattering calculations," *IEEE Transactions on Microwave Theory and Techniques*, Vol. 39, No. 4, 638–642, Apr. 1991.

8. Christopoulos, C., *The Transmission-line Modeling Method,* IEEE Press, NJ, 1995.
9. Christopoulos, C., *The Transmission-line Modeling (TLM) Method in Electromagnetic,* Morgan and Claypool Publishers, CO, 2006.
10. Jin, H. and R. Vahldieck, "Direct derivations of TLM symmetrical condensed node and hybrid symmetrical condensed node from Maxwell's equations using centered differencing and averaging," *IEEE Transactions on Microwave Theory and Techniques*, Vol. 42, No. 12, 2554–2561, Dec. 1994.
11. Jin, H. and R. Vahldieck, "A new frequency-domain TLM symmetrical condensed node derived directly from Maxwell's equations," *IEEE Transactions on Microwave Theory and Techniques International Symposium*, Vol. 2, 487–490, 1995.
12. Raveu, N., T. P. Vuong, I. Terrasse, G.-P. Piau, G. Fontgalland, and H. Baudrand, "Wave concept iterative procedure applied to cylinders," *IEE Proceeding on Microwave Antenna and Propagation*, Vol. 151, No. 5, 409–416, Oct. 2004.
13. Wane, S., D. Bajon, H. Baudrand, and P. Gammand, "A new full-wave hybrid differential-integral approach for the investigation of multilayer structures including nonuniformly doped diffusions," *IEEE Transactions on Microwave Theory and Techniques*, Vol. 53, No. 1, 200–214, 2005.
14. N'gongo, R. S. and H. Baudrand, "A new approach for microstrip active antennas using modal F.F.T-algorithm," *IEEE Antennas and Propagation Society International Symposium*, Vol. 3, 1700–1703, 1999.
15. Sadiku, M. N. O., *Numerical Techniques in Electromagnetics,* 2nd Edition, CRC Press, 2001.
16. Hesselbarth, J., "Passive microwave circuit elements analyzed with the frequency-domain TLM method," Thesis of Doctor of the Swiss Federal Institute of Technology Zurich, 2002.
17. Azizi, M., H. Aubert, and H. Baudrand, "A new iterative method for scattering problems," *Proceedings of the European Microwave Conference*, 255–258, 1995.
18. Zugari, A., M. Khalladi, M. I. Yaich, N. Raveu, and H. Baudrand, "New approach: WCIP and FDTLM hybridization," *2009 Mediterranean Microwave Symposium (MMS)*, 1–4, 2009.
19. Glaoui, M., H. Trabelsi, H. Zairi, A. Gharsallah, and H. Baudrand, "A new computationally efficient hybrid FDTLM-WCIP method," *International Journal of Electronics*, Vol. 96, No. 5, 537–548, 2009.

20. Raveu, N. and O. Pigaglio, "Résolution de problèmes hautes fréquences par les schémas equivalents cours et exercices corrigés," Editions Cépaduès, Apr. 2012.
21. Girard, C., N. Raveu, R. Perrussel, and S. Lanteri, "Hybridation entre la WCIP et des méthodes volumiques," *Journées Nationales Microondes (JNM)*, May 2013 (in French).
22. Nguyen, N. C., J. Peraire, and B. Cockburn, "Hybridizable discontinuous Galerkin methods for the time-harmonic Maxwell's equations," *Journal of Computational Physics*, Vol. 230, No. 19, 7151–7175, Aug. 2011.